BAYESIAN SEA ICE DETECTION WITH ASCAT

Jeroen Verspeek[(1)], Maria Belmonte Rivas[(2)] , Ad Stoffelen[(1),], Anton Verhoef[(1),], Jur Vogelzang[(1)]

[(1)] *KNMI, Postbus 201, 3730 AE de Bilt, the Netherlands*, Email:verspeek@knmi.nl, stoffele@knmi.nl
[(2)] *NCAR, P.O. Box 3000, Boulder, CO 80307, USA ,* Email: rivasm@ucar.edu

ABSTRACT

A sea ice model for the Advanced Scatterometer (ASCAT) onboard Metop-A satellite has been developed. The conditional probabilities for sea ice and wind are combined with a priori information in a Bayesian algorithm resulting in a posterior ice/wind probability. The Bayesian sea ice extent from ASCAT is compared against other sea ice detection algorithms for active and passive microwave instruments, most notably Quikscat and the Advanced Microwave Scanning Radiometer (AMSR).

The algorithm constitutes a useful tool for sea ice discrimination and helps in the quality control of the wind retrieval procedure. Moreover, the resulting sea ice maps provide relevant information on the state of the ice pack and its seasonal dynamics.

1. INTRODUCTION

Every Wind Vector Cell (WVC) of ASCAT is illuminated by three antenna beams at different azimuth and incidence angles, forming a triplet $\{\sigma^0_{fore}, \sigma^0_{mid}, \sigma^0_{aft}\}$. Fig.1 shows the observation geometry for ASCAT.

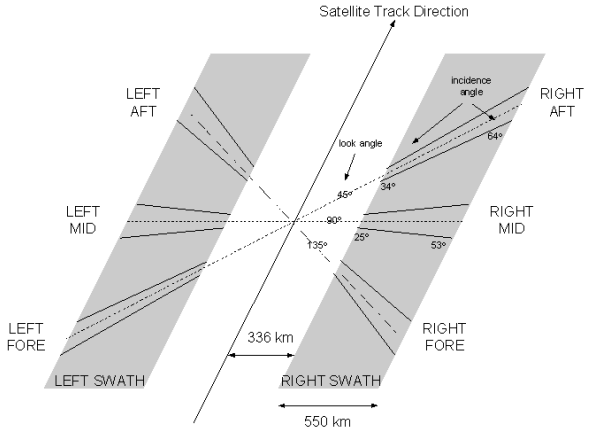

Figure 1 – ASCAT observation geometry (courtesy EUMETSAT)

The triplets may be visualized in a 3-dimensional measurement space, where the axes represent the backscatter values of the fore, aft and mid antenna [1]. For a given WVC number, i.e., position across the swath, it is shown that ocean backscatter triplets are distributed around a well-defined "conical" surface. The signal largely depends on just two geophysical parameters, i.e., wind speed and direction.

A sea ice model for the Advanced Scatterometer (ASCAT) onboard Metop-A satellite has been developed following an approach elaborated earlier for the ERS scatterometers. The newly developed sea ice model for ASCAT describes the statistical distribution of sea ice (triplet) points in the 3D-measurement space at each WVC, which conforms to a straight line in this 3D space. This line constitutes an empirical Geophysical Model Function (GMF) for sea ice in the same sense that the wind cone is an empirical GMF for ocean winds [1]. Like the projection of a measurement triplet on the wind cone gives information on the wind speed and wind direction, the projection of a triplet on the ice line gives information on the ice type (e.g. first-year or multi-year ice). The distance of a measurement triplet to the ice line is translated into a conditional probability for sea ice, in the same way that the distance of this triplet to the wind cone becomes a conditional wind probability.

The conditional probabilities for sea ice and wind are combined with a priori information in a Bayesian algorithm resulting in a posterior ice/wind probability. Different space- and time-averaging schemes can be applied to reduce the number of wrongly classified triplets. Background ECMWF wind information is also used in the Bayesian algorithm. The use of Sea Surface Temperature (SST) can help for a quick initialisation of the ice algorithm but is not used in the results presented here.

The sea ice extent from the ASCAT sea ice model is compared against existing sea ice detection algorithms for the active respectively passive microwave instruments QUIKSCAT and AMSR.

2. SEA ICE MODEL FOR ASCAT

The empirical method used to derive a wind GMF in 3D measurement space can be applied to define a sea ice GMF. It has the advantage that no a-priori assumptions on the ice model need to be made and that the full information content of the measurements is used. We applied this method to the ERS [2] and to the ASCAT

Proc. 'ESA Living Planet Symposium', Bergen, Norway
28 June – 2 July 2010 (ESA SP-686, December 2010)

scatterometers [3]. Plots of measured triplets in measurement-space show that for each WVC all ice points lie on a straight line in the plane $\sigma^0_{fore} = \sigma^0_{aft}$, implying azimuthal isotropy of sea ice backscatter.

This means that for a particular WVC (fixed incidence angles θ) the sea ice backscatter is only dependent on a scalar a, defining the triplet position along a tilted ice line. For convenience, for each WVC a sea ice coordinate system is defined ($\mathbf{e}_a$, $\mathbf{e}_b$, $\mathbf{e}_c$). The ice coordinates are denoted (*a, b, c*), where *a* represents the position along the ice line, and *b* and *c* the distances to the ice line across and along the symmetry plane $\sigma^0_{fore} = \sigma^0_{aft}$. The ice line is represented by:

$$\boldsymbol{\sigma}^0(a) = \mathbf{O} + a\mathbf{e}_a \qquad (1)$$

The abscissa along the ice line *a* represents the strength of backscatter, which can be used as a proxy for ice type or sea ice age. The distance to the ice line d_{ice} is defined as:

$$d_{ice} = \sqrt{\frac{1}{2}(b^2 + c^2)} \qquad (2)$$

The origin **O** of the ice line is chosen to coincide with the mean backscatter for a large collection of triplets using a conservative ice mask, so that all measurements are certainly representing sea ice. As a result of this procedure the mean values of *a*, *b*, and *c* will be zero. Then the direction of the ice line $\mathbf{e}_a$ is determined using the collection of measurement triplets. Scaling factors are applied for coordinates *b* and *c*, so that the distance to the ice line is always measured in units of the standard deviation of *b* and *c*. To the *a*-coordinate in every WVC a scaling factor is applied that matches the standard deviation of the WVC in the middle of the swath. In this way the value of the *a*-coordinate will have the same physical meaning independent of the WVC.

In Fig.2a the wind cone and sea ice line are depicted in measurement space together with some measurement triplets.

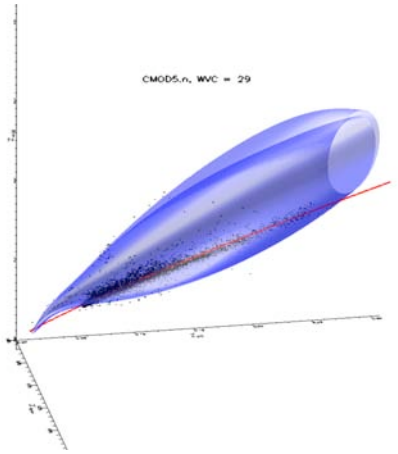

Figure 2a - Wind cone (blue) and ice line (red) in measurement-space. Backscatter triplets are shown as black dots.

Fig.2b shows 2D-views on the wind cone and ice line for several WVCs together with probability contours for ice measurements. Note that for the outer swath the ice line is lying inside the wind cone, and for the inner swath outside the cone. For some mid swath WVCs the ice line is close to the part of the wind cone that corresponds to cross winds, which may hinder an effective discrimination.

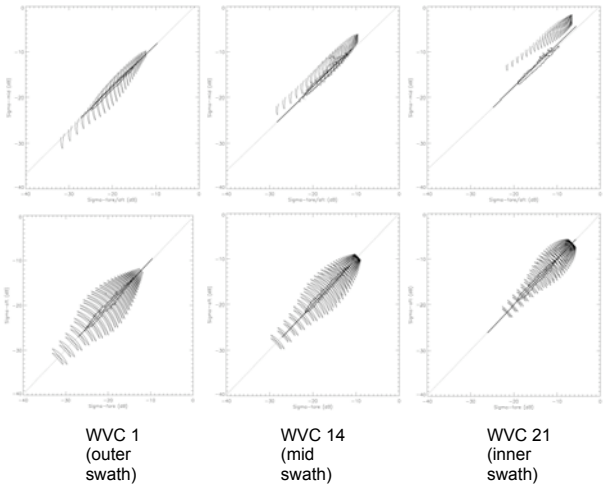

Figure 2b – Side views across the $\sigma^0_{fore} = \sigma^0_{aft}$ symmetry plane and top views of the wind cone and ice line. Probability contour intervals for ice measurements are also shown.

3. BAYESIAN PROBABILITY PROPAGATION

Bayesian statistics are used in decision theory, where you have a set of measurements and a number of "classes" into which the measurements can be categorized. When the a priori probability of each class is given, as well as an expected probability distribution of measurements error model for each class, the a

posteriori probability that a measurement belongs to a certain class can be calculated using Bayes' theorem. In our model we assume there are only two classes, *ice* and *water*, with a priori probabilities *P(ice)* and *P(water)* and a posteriori probabilities $p(ice|\boldsymbol{\sigma^0})$ and $p(water|\boldsymbol{\sigma^0})$ ($\boldsymbol{\sigma^0}$ stands for a scatterometer triplet).

The expected probability distribution of backscatter triplets for the *water* class, $p(\boldsymbol{\sigma^0}|water)$ is modeled as a function of the Maximum Likelihood Estimate (MLE) or distance to wind cone. The MLE follows a normal distribution function.

Optionally an extra error model can be used where the vector distance between the scatterometer retrieved wind and the collocated ECMWF background wind is assumed to have a Gaussian distribution in both components. This option is used for the results presented here but it turned out that the effect on the ice classification is only small.

The expected probability distribution of backscatter triplets for the *ice* class, $p(\boldsymbol{\sigma^0}|ice)$ is modeled as a function of the distance to the ice line d_{ice} in Eq.2. The *b* and *c* ice coordinates follow a normal distribution function thus d_{ice} follows a Rayleigh distribution function.

Because there are only these two classes, the following holds true:

$$\begin{aligned} P(ice)+P(water) &= 1 \\ p(ice|\sigma^0)+p(water|\sigma^0) &= 1 \end{aligned} \qquad (3)$$

The posterior probability of ice $p(ice|\boldsymbol{\sigma^0})$ is now given by Bayes' theorem

$$p(ice\,|\,\sigma^0) = \frac{P(ice)\,p(\sigma^0\,|\,ice)}{P(ice)\,p(\sigma^0\,|\,ice)+P(water)\,p(\sigma^0\,|\,water)} \qquad (4)$$

Which can be rewritten using eq. 3 and the function *Logit(p)*: = *log(p/(1-p))* into:

$$Logit\left(p(ice\,|\,\sigma^0)\right) = Logit\left(P(ice)\right)+\ln\left(\frac{p(\sigma^0\,|\,ice)}{p(\sigma^0\,|\,water)}\right) \qquad (5)$$

Eq.5 is used to propagate the posterior ice probability.

3.1. Time relaxation of the prior ice probability

The prior probability $P_n(ice)$ at time t_n is calculated using the posterior probability $p(ice|\boldsymbol{\sigma^0}_{n-1})$ at time t_{n-1} of the previous measurement, and a climatology value $P_{cl}(ice)$:

$$P_n(ice) = P_{cl}(ice)^{[1-w_n(t_{n-1})]}\, p(ice\,|\,\sigma^0{}_{n-1})^{w_n(t_{n-1})}$$

where $w_n(t_i)$ is an exponentially decaying weight function with decay time *A*:

$$w_n(t_i) = \exp\left(-\frac{(t_n - t_i)}{A}\right) \qquad (6)$$

It can be shown that $P_n(ice)$ is always lying in between $P_{cl}(ice)$ and $p(ice|\boldsymbol{\sigma^0}_{n-1})$.

If the time between two measurements t_n and t_{n-1} is very large then $w_n(t_{n-1}) \rightarrow 0$ and the prior probability $P_n(ice) \rightarrow P_{cl}(ice)$. The information of the previous measurement is lost and the climatology value is used as the a priori probability.

If the time between two measurements t_n and t_{n-1} is very short then $w_n(t_{n-1}) \rightarrow 1$ and the a priori probability $P_n(ice) \rightarrow p(ice|\boldsymbol{\sigma^0}_{n-1})$. The information of the previous measurement is still valid and it is used as prior probability.

3.2. Space-time relaxation of the posterior ice probability

The ice probability is stored for the North pole and South pole region using a polar stereographic grid with pixel dimension of 12.5x12.5 km^2. This grid has a finer granularity than the ASCAT swath data that has a WVC dimension of 25x25 km^2 in nominal mode. The posterior ice probability $p(ice|\boldsymbol{\sigma^0})$ is spatially averaged using a 7x7 subgrid. The spatial averaging ensures that the available information is spread across the grid according to the measurement resolution.

A Gaussian distribution is used as a spatial weighting function, and the exponential decay function from Eq.6 is used as a time weighting function:

$$W(r,t) \sim \exp(-(r/L)^2)\exp((-\Delta t/A)) \qquad (7)$$

Here *r* is the distance from the neighboring pixel to the central pixel, *L* is a decay length. Δt is the time difference between the measurement time at the neighboring pixel and the measurement time at the central pixel. After normalization this weighting function is used to calculate an averaged posterior ice probability.

4. COMPARISON OF SEA ICE EXTENT WITH QUIKSCAT AND AMSR

The sea ice extent from ASCAT has been compared with sea ice extents from the Quikscat scatterometer and the AMSR passive radiometer over 2008. The ASCAT algorithm was run starting from 2007-12-16 so that the ice map had two weeks to form and initialisation effects could be ruled out. AMSR-E ice maps were taken from Aqua from the EOS data gateway. This 12.5 km sea ice concentration product is generated using the Enhanced NASA Team (NT2) algorithm [4]. The Quikscat algorithm has been developed and used operationally at KNMI [5, 6]. It also uses an empirical ice GMF in combination with a Bayesian probability propagation.

As an example in Fig.3 the Antarctic sea ice extent for ASCAT and Quikscat is shown for 2008-06-07, and in Fig.4 the Arctic sea ice extent for ASCAT and AMSR. The sea ice parameter *a*-coordinate is shown in grayscale. For ASCAT the green pixels represent a low number of measurements, and orange pixels represent ice, but with the standard deviation of the *a*-coordinate above a certain value. The orange value can indicate rapid changes in ice properties, e.g. melt. As can be seen in Fig.3 the Quikscat ice map shows more detail because no spatial averaging is used, only a temporal relaxation is applied. The swath of Quikscat is wider than the ASCAT swath which results in a higher sampling rate. Another difference is in the wavelength of the radar, Quikscat uses Ku-band compared to C-band for ASCAT. The Ku-band gives a high absolute backscatter for sea ice and the distinction in absolute backscatter value between ice and water is always large. This fact can be used for an effective ice-water discrimination. The ASCAT C-band backscatter for sea ice and water are comparable in some cases which may hinder an effective discrimination.

In Fig.3c the difference between ASCAT and Quikscat is shown, based on a 50% ice probability threshold for both scatterometers. The red area represents (ASCAT=ice and Quikscat=not ice) and blue area represents (Quikscat=ice and ASCAT=not ice). For this date the agreement is very good.

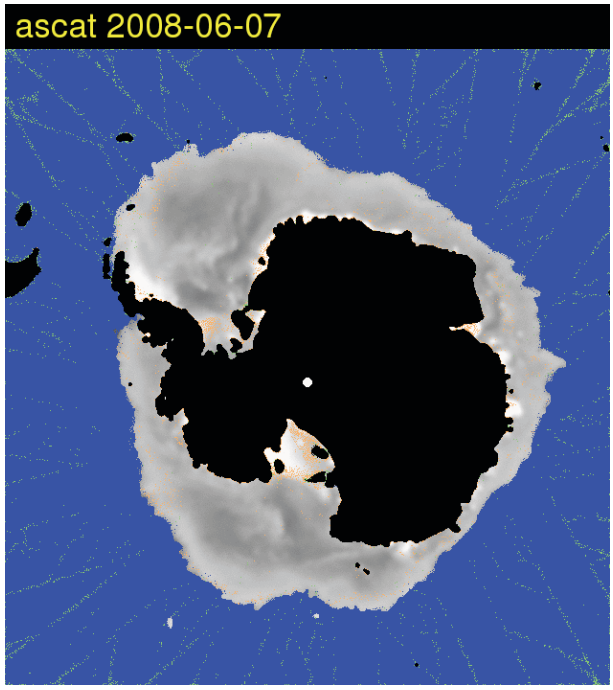

Figure 3a - ASCAT sea ice for the Antarctic region. The ice a-coordinate is shown in greyscale.

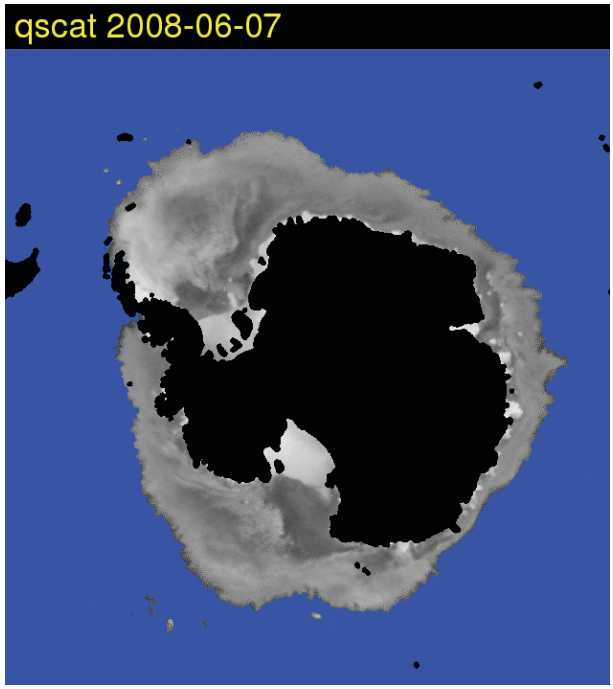

Figure 3b - Quikscat sea-ice for the Antarctic region. The ice a-coordinate is shown in greyscale.

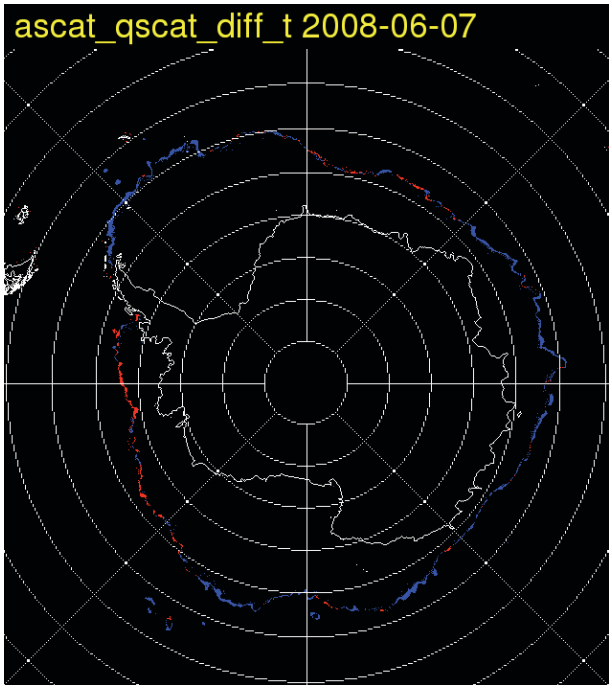

Figure 3c - Difference between ASCAT and Quikscat sea-ice extent based on the 50% probability threshold. Red: (ASCAT=ice and Quikscat=not ice) Blue: (Quikscat=ice and ASCAT=not ice)

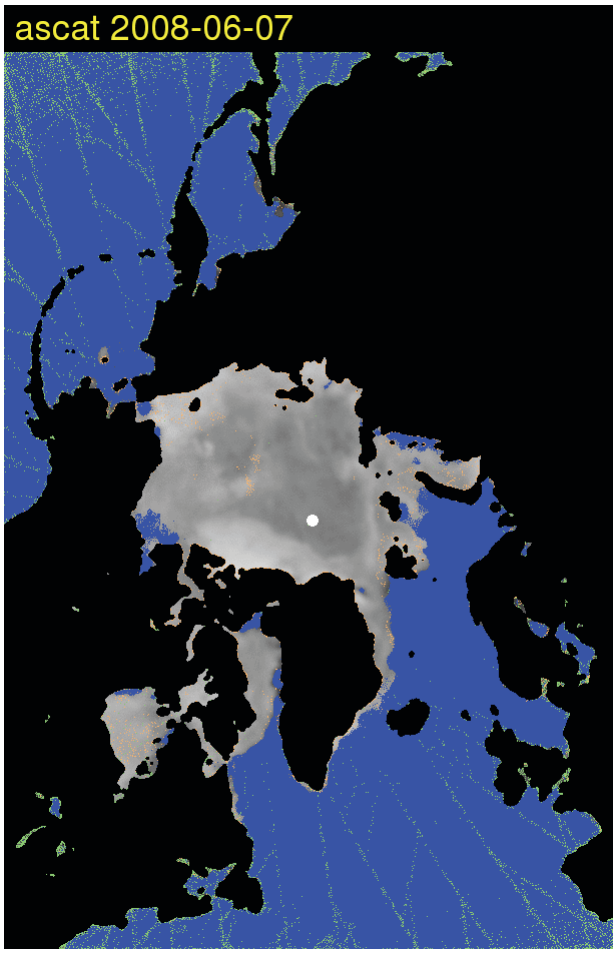

Figure 4a - ASCAT sea-ice for the Arctic region. The ice a-coordinate is shown in greyscale.

In Fig.4 the Arctic sea-ice extent is shown for ASCAT and AMSR on 2008-06-07.

AMSR is a passive radiometer and has a higher spatial resolution than a typical scatterometer. Shown is the ice concentration in greyscale. Following [5, 6] a AMSR 15% ice concentration matches best with Quikscat 50% ice probability so the 15% threshold is used for the sea-ice extent comparison between ASCAT and AMSR in Fig.4c. Note that some green areas near the European and Canadian coast are falsely classified as ice. This will give a overestimation of the total sea-ice area for ASCAT.

Figure 4b - AMSR sea-ice for the Antarctic region. The ice concentration is shown in greyscale

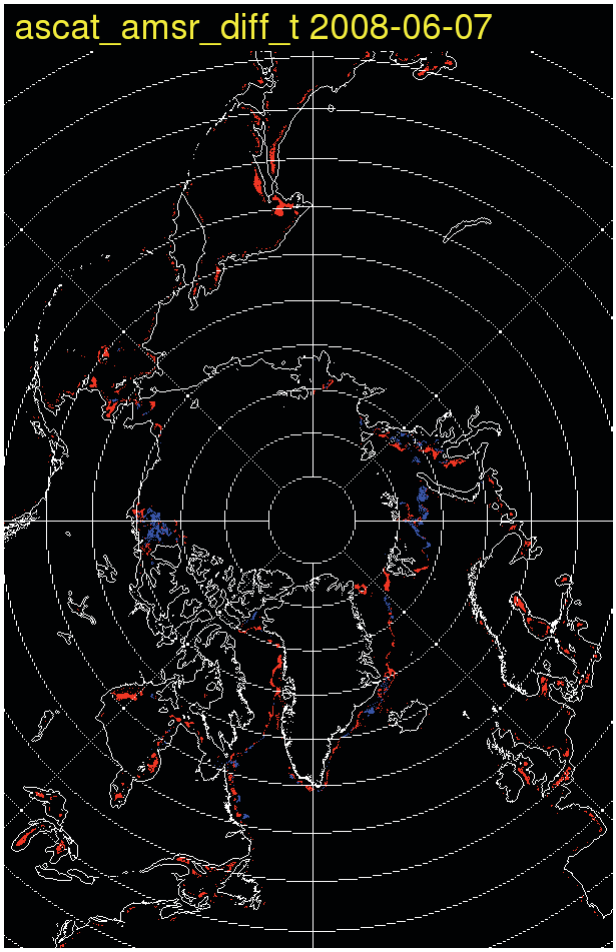

Figure 4c - Difference between ASCAT and AMSR sea-ice extent based on the 50% probability threshold for ASCAT and a 15% ice concentration for AMSR. Red: (ASCAT=ice and AMSR=not ice) Blue: (AMSR=ice and ASCAT=not ice)

In Fig.5 the total sea ice is plotted for the whole year of 2008 for the three sensors. The land masks and missing data points are mutually applied in order to get a fair comparison between the three. Fig.5a shows the Arctic region and Fig.5b the Antarctic region respectively.

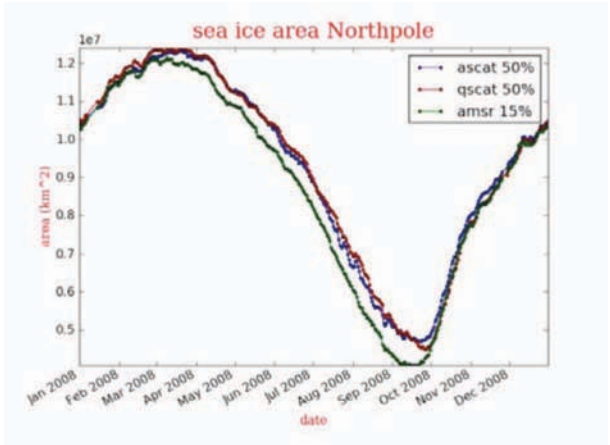

Figure 5a – Total sea ice area for the Arctic region in 2008 for the three sensors ASCAT, Quikscat and AMSR.

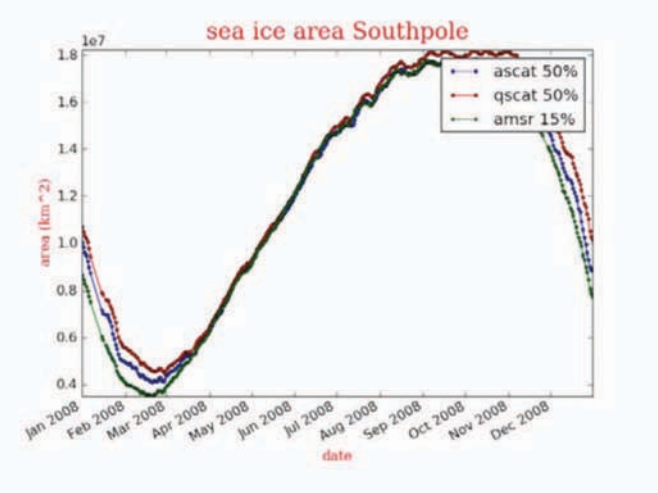

Figure 5b – Total sea ice area for the Antarctic region in 2008 for the three sensors ASCAT, Quikscat and AMSR.

As can be seen the agreement in the periods of ice growth is remarkably good. During ice melt periods the agreement is less good in general because mixed states where areas are partly water and partly ice occur. These mixed states are not modelled by the ASCAT and Quikscat GMFs and the Bayesian approach does not take them into account either. Therefore the mixed states are harder to grasp.

For the Arctic melt season the agreement between ASCAT and Quikscat is excellent pointing at deficiencies in the summer sea ice extents as observed by AMSR. For the Antarctic melt season ASCAT is somewhere between the values of AMSR and Quikscat.

5. CONCLUSIONS

The ASCAT sea ice model in combination with Bayesian probability propagation provides good preliminary results. A comparison with Quikscat and AMSR shows good agreement especially during the ice growth periods. During ice melting periods the agreement with Quikscat is still good with some larger deviations from AMSR. Some spurious ice classification by ASCAT near coastal regions in the Arctic region has to be worked on. The ASCAT ice model is running in experimental mode at KNMI. When using a conservative ice mask, e.g., a 30% ice probability, the ASCAT ice model can be used as an alternative to the presently used SST-based sea ice screening for the level 2 wind product.

6. OUTLOOK

Spatial coverage of ASCAT is poorer than that of Quikscat which has a broader swath. METOP-B, to be

launched in 2012 with a second ASCAT instrument, would help to achieve a better spatial coverage. The combined data from both instruments can be used to build a common ice map.

We expect ASCAT and QuikSCAT algorithms can be brought to a better agreement both during the growth and melt seasons. Given their high sensitivity to diffuse sea ice conditions, scatterometers have high potential for sea ice detection.

7. ACKNOWLEDGEMENT

Scatterometer research and development, and routine processing and monitoring [7] at the Royal Netherlands Meteorological Institute (KNMI) are funded by EUMETSAT through the Satellite Application Facilities (SAF). More specifically, the work on sea ice is part of the Ocean and Sea Ice (OSI) SAF [8].

REFERENCES

1. Stoffelen, A. (1998), Scatterometry, thesis Un,. Utrecht, the Netherlands

2. de Haan, S. & Stoffelen, A. (2001), Ice discrimination using ERS scatterometer, KNMI, *OSISAF report*, de Bilt, the Netherlands

3. Verspeek, J. (2006), Sea ice classification using Bayesian statistics, *KNMI report*, de Bilt, the Netherlands

4. Markus, T. and Cavalieri D.J., An enhancement of the NASA Team sea ice algorithm, *IEEE Trans. Geoscience Remote Sensing*, 38, 1387-1398, 2000

5. Belmonte Rivas, M., Stoffelen, A., Near Real-Time sea ice discrimination using SeaWinds on QUIKSCAT, *OSISAF Visiting Scientist report*, de Bilt, the Netherlands, SAF/OSI/CDOP/KNMI/TEC/TN/168, 2009

6. Belmonte Rivas, M., Stoffelen, A., A Bayesian algorithm for sea ice detection with QUIKSCAT (*submitted to TGARS*), 2010

7. KNMI scatterometer web site (2010), http://www.knmi.nl/scatterometer

8. Ocean & Sea Ice web site (2010), http://www.osi-saf.org